



OPEN Pulsed electric field ablation process—the effect of bifurcation stents on electric field and heat distribution

Zhen wang^{1,2}, Jingyang Sun¹✉, Ming Liang^{1,3}, Jie Zhang¹, Yulai Yan¹, Fengqi Xuan⁴, Lisheng Xu⁵ & Yaling Han^{1,3}✉

Pulsed field ablation (PFA) is a novel non-thermal technique for arrhythmia treatment, capable of targeting the epicardium. However, the effects of coronary bifurcation lesions (BL) and bifurcation stents (BS) on ablation efficacy have not been evaluated. A three-dimensional computer simulation model was developed to assess the effect of the ablation region. The ablation catheter was set to be located directly above the BS model by performing a true size reduction of the ablation device. The ablation region was evaluated using an electric field strength contour of 1000 V/cm. The influence of coronary BL and BS on PFA ablation efficacy was assessed using ablation effect maps from different models. BS did not induce electric field coupling, and the distortion of the electric field in the ablation region remained unchanged, with cold and hot spots located similarly. The presence of coronary branches reduced the ablation area width, with a maximum difference of 2.82 mm. The angle between the ablation catheter and the main coronary artery branch had a smaller effect on the ablation zone width, with a maximum difference of 1.24 mm. The presence of BS will have a positive effect on the temperature increase in the ablation region (3.59 °C temperature increase in the presence of BS). The results indicate that BL and BS influence the electric field distribution in the ablation region. However, this distortion is confined to the ablation area, with no coupling between the main coronary artery and its branches to exacerbate the electric field distortion. The presence of BS exacerbates the temperature rise at the ablation site, but this increase does not cause thermal damage to the region.

Keywords Pulsed electric field, Arrhythmia, Coronary artery, Bifurcation lesion, Bifurcation stent, Computer modeling

Pulsed field ablation (PFA) has recently emerged as a novel treatment for arrhythmias. PFA is a non-thermal ablation technique that treats arrhythmias by applying a high-voltage electric field to the target site, disrupting cellular homeostasis and causing cell death^{1–5}. Arrhythmias, particularly atrial fibrillation and supraventricular tachycardia, significantly affect quality of life and increase the risk of complications such as arterial embolism and stroke^{6,7}. Studies have shown that the ganglionic plexus in the epicardial fat layer plays a key role in the induction and maintenance of arrhythmias. Computational models suggest that the ganglionic plexus contributes to the distribution of the electric field in PFA, likely due to its higher electrical conductivity compared to surrounding adipose tissue^{8,9}. Subsequent studies proposed that coronary metal stents have higher electrical conductivity than ganglion plexuses, which may exacerbate electric field distortion and increase the temperature in the ablation region. Hogenes et al. found in their experiments with PFA on tumors that metal stents near the ablation electrodes distort the normal electric field. Follow-up studies further revealed that the presence of metal stents increased the temperature at the ablation target site^{10–12}.

Ana et al. developed a two-dimensional computational model and found that the presence of a metallic stent in a coronary artery causes a normal electric field distribution in the ablation region, while the metal's properties increase the region's temperature. However, this temperature change does not cause thermal damage

¹Department of Cardiology, General Hospital of Northern Theater Command, Shenyang, China. ²College of Medicine and Biological Information Engineering, Northeastern University, Shenyang, China. ³National Key Laboratory of Frigid Zone Cardiovascular Diseases, Shenyang, China. ⁴Department of Cardiology, Tianjin Chest Hospital, Tianjin, China. ⁵College of Information Science and Engineering, Northeastern University, Shenyang, China. ✉email: sjy2006411039@sina.com; hanyaling@163.net

to surrounding tissues. Researchers later developed simplified models of the ablation area based on the human body's real three-dimensional structure and compared these with complex models. This comparison reduced the complexity of 3D modeling while minimizing the gap between the models in terms of ablation area and depth^{13,14}. Coronary bifurcation lesions (BL) are common in clinical practice. It has been shown that coronary metallic stents cause electric field distortions and thermal changes at the PFA targeting site. However, the effects of bifurcated stents (BS) on the electric field and temperature distribution during pulsed ablation have not been fully evaluated (BL are atherosclerotic lesions within the coronary arteries that occur at the bifurcation of the vessel.). Therefore, to address this, we conducted multi-angle computer modeling of BS to assess the differences in electric field and temperature distributions across various models. This study aims to enhance the application of pulsed-field ablation for arrhythmia treatment in clinical practice.

Methods

Computational modeling

To analyze and compare the effects of bifurcation lesions and bifurcation stents on pulsed electric field ablation, we used a three-dimensional computational model. In the model, we focused solely on the area containing the ablation device and its potential effects, a simplification method supported by previous studies^{14–16}. We realistically scaled the ablation device dimensions in the model and layered it according to the above conclusions. Based on the real structure of the human heart, the regions of interest (saline, fat, coronary arteries, myocardium, and blood) were modeled in distinct layers. To simulate a real ablation scenario, the device was placed above the fat layer^{9,13,17}. The ablation model is shown in Fig. 1.

The ablation electrode diameter was set to 3.98 mm, with a width of 2.56 mm, and the distance between electrodes was 6.23 mm. A saline layer was included in the model to serve primarily to cool the temperature and homogenize the electric field. To ensure effective energy transfer to the region of interest, the ablation electrodes were fully attached to the fat layer in the computational model^{14,18–21}. In the model, the fat thickness was 4.3 mm, myocardium thickness 2.7 mm, and blood thickness 40 mm. The model's length and width were set to 80 mm and 40 mm, respectively, based on previous studies^{9,22,23}. For the metal stent, we set the outer diameter of 2.5 mm and the wall thickness of 0.1 mm. In order to facilitate the calculation and analysis, we used the same design parameters for both metal stents in the simulation^{24,25}. The vessel diameter was kept constant for simplification in this simulation. The impact of bifurcation lesion location on ablation areas was also considered. Different sections of the computational model were studied. The ablation model is shown in Fig. 2. In this simulation, the vessel diameter was kept constant for simplification, and different locations of bifurcation lesions were considered to assess their impact on the ablation area. We have studied different cross sections of the computational model.

Pulse parameters and boundary conditions

Boundary conditions were set for the computational simulation model. In the computational model, two pulse widths were used: 1000 V for the ablation electrode, with a pulse time and interval of 100 μ s each. To compare the effect of different pulse widths on the ablation area, a second simulation was run with 1000 V, 50 μ s pulse time, and 50 μ s pulse interval. The total ablation time was kept constant in the computational model to analyze whether the pulse width affects the ablation area^{14,18,26}. The computational model is set to 0 V for the dispersed electrode and 0 for the other model surface currents, which indicates that the ablation energy propagates only between the ablated and dispersed electrodes^{13,14}. The energization time for this simulation was 2 ms, and the specific ablation pulse parameters are shown in Fig. 3.

To evaluate the effect of pulsed electric field ablation on the temperature of the ablation region, we set the thermal boundary conditions for the computational model. To analyze the effect of different pulse widths on the temperature of the ablation region, we applied Newton's law of cooling to set the air-electrode interface parameter at 20 W/m²·K (ambient temperature: 21 °C). The myocardium-blood interface was set with a thermal convection coefficient of 1417 W/m²·K to simulate the effect of thermal convection on the temperature, with an

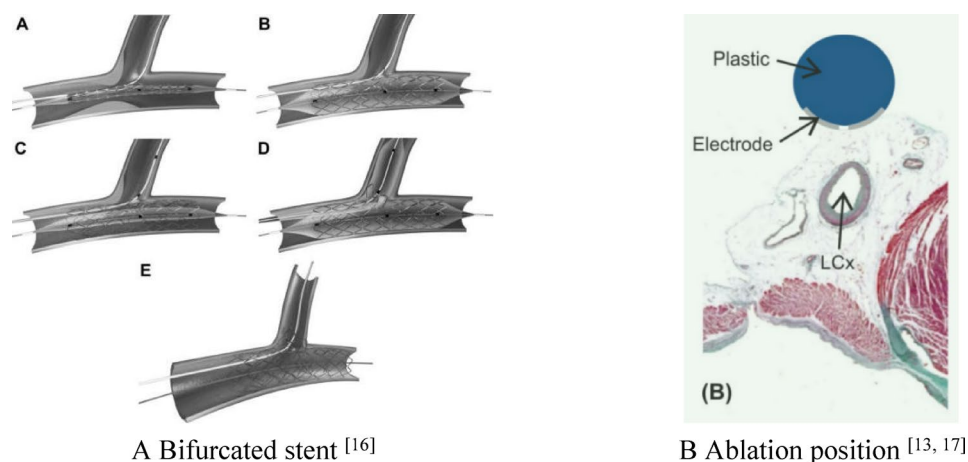


Fig. 1. Schematic diagram of human ablation area.

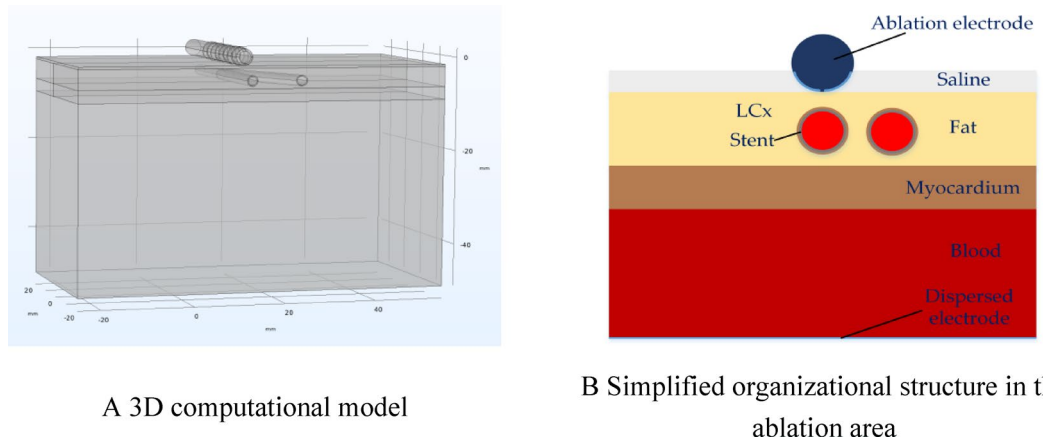


Fig. 2. Schematic diagram of the computational model^{13,14}.

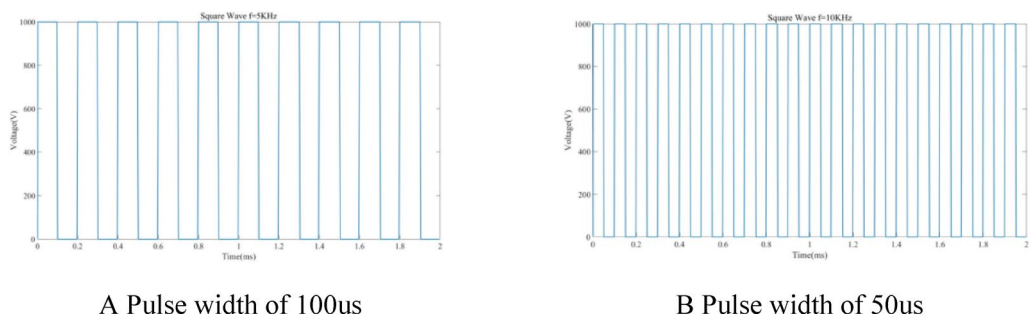


Fig. 3. Pulse parameters.

endocardial blood flow velocity of 24.4 cm/s at a tissue temperature of 37 °C^{27,28}. In the simulation, we compared coronary artery bifurcation lesions, with a blood flow rate of 0.5 m/s, thermal convection coefficient of 63.19 W/m²·K, and blood viscosity coefficient of 0.0021 kg/(m·s)^{29,30}.

Controlling equations and material properties

Based on the above analysis, the pulsed electric field ablation model is an electro-thermal coupling problem. To address this electro-thermal coupling problem, we established a three-dimensional computational model in the finite element analysis software COMSOL (COMSOL Multiphysics[®]. Version 5.5. COMSOL AB, Stockholm, Sweden.). The specific model parameters are shown above, and a tetrahedral mesh was used for the model structure. In the model, the catheter electrode is placed in the saline layer to simulate its real clinical position. As this is an electro-thermal coupling problem, we included the biological heat transfer module in the model. Additionally, Laplace’s equation was used to simulate the pulsed ablation electric field^{31–33}.

$$\begin{cases} J = \sigma E \\ E = -\nabla V \\ \nabla \cdot (\sigma \nabla V) = 0 \end{cases}$$

Where σ is conductivity (S/m), V is voltage, E is electric field strength (V/m), and J is current density (A/m²). The phenomenon of tissue temperature rise in the target region caused by PFA during epicardial ablation was considered using the bioheat Eqs^{27,34}.

$$\begin{cases} Q = \sigma |E|^2 \\ \rho c_p \frac{dT}{dt} = \nabla \cdot (k \nabla T) + Q + Q_e + Q_{met} \end{cases}$$

Where ρ is the density (kg/m³), c is the specific heat (J/kg·K), T is the temperature (°C), t is the time (s), k is the thermal conductivity of the tissue (W/m·k), Q is the heat source generated by the electric field (W/m³), Q_p is the heat loss due to the blood flow (W/m³), and Q_{met} is the heat loss due to the biological metabolism (W/m³).

In the model calculation, we assign appropriate conductivity values to different tissues due to their distinct cellular structures, which affect conductivity. Proper conductivity parameter design ensures more accurate model results. Researchers have found that the conductivity of biological tissues changes during PFA ablation due to electroporation, which enhances current penetration. In order to accurately simulate the temperature

Mlement	Saline	Blood	Myocardium	Fat	Electrode	Stent	Poyurethane
k(W/m-K)	0.628	0.52	0.56	0.21	71	15	23
c(J/kg-K)	4184	3617	3686	2348	132	480	1050
ρ (kg/m ³)	980	1050	1081	911	21,500	8000	1440

Table 1. Control equations and parameters for bioheat calculations.

Mlement	Stent	Electrode	Poyurethane	Saline	Myocardium	Blood	Fat
σ_0 (S/m)	7.4e ⁶	4.6e ⁶	1e ⁻⁵	1.392	0.0537	0.7	0.0377
σ_1 (S/m)					0.281	0.748	0.0438

Table 2. Parameters for model conductivity calculation.

changes in the ablation region, we used a pair of pulse waveform simulations for the biothermal simulation calculations^{13,35}. In this study, we use a Sigmoid function to model these conductivity changes. Additionally, temperature changes slightly affect conductivity, so we set the conductivity of saline, blood, and other substances to increase by 2% with temperature^{36–38}. In the simulation, we use 0 and 1 to represent tissue conductivity before and after electrical stimulation, with values changing as tissue voids form. Relevant parameters are shown in Tables 1 and 2^{13,36,39,40}. The parameters we used in this simulation were obtained from previous studies.

$$\sigma(E, T) = \left(\sigma_0 + \frac{\sigma_1 - \sigma_0}{1 + 10e^{-\frac{(|E| - 58,000)}{3000}}} \right) \cdot 1.02^{T-37}$$

Here, σ_0 and σ_1 represent the conductivity before and after electroporation, respectively, with their values being related to the presence and size of pores in the cell membrane. Before electroporation occurs, when pores have not yet formed, current flows only through the extracellular material, similar to low-frequency electrical excitation where the cell membrane acts as an electrical insulator. Under practical conditions, this effect remains stable between 1 and 10 kHz. At higher pulse frequencies, conductivity in the myocardium decreases due to pore formation, allowing current to flow not only extracellularly but also through the cytoplasm. However, the regional effect of PFA ablation remains negligible at other pulse frequencies^{14,36}.

Analysis of results

There are several types of coronary BL, and BS provides a solution for this lesion. The effect of BS on the pulsed electric field ablation area has not been thoroughly evaluated in arrhythmia treatment protocols. In this paper, we simulate and analyze cases using the finite element simulation software COMSOL to assess pulsed electric field ablation near the BS, including electric field distribution and temperature effects in the ablation area. Computational simulations were conducted for various scenarios, including different pulse widths, BS locations, distances between the ablation catheter and coronary artery, and the presence or absence of a metallic stent. We used an electric field contour of 1000 V/cm in the simulations to assess the depth and width of the ablation region, as studies have shown that a pulsed electric field at this threshold can cause irreversible myocardial damage^{16,41,42}. Temperature simulations were conducted to evaluate potential adverse thermal effects induced by the BS during ablation. The total duration of the simulation was kept consistent (as shown in Fig. 2), and the ablation duration was the same for both pulse widths to assess their impact on the temperature of the ablation region.

Results

Electric field distribution

Coronary artery BL is a lesion characterized by severe stenosis of the main coronary artery and its branches, either separately or simultaneously. To analyze its effect on pulsed electric field ablation in greater detail, we first assume that no BS is present at the lesion site. Then, we classify the lesion into two types based on the distance of ablation catheter and the coronary artery (1 mm and 1.5 mm, respectively). The calculations for these two lesion types are performed first in this study. Specifically, three cross-sections are selected for computational modeling: A and D, B and E, and C and F each correspond to the same section. Section A is the section in which only the main coronary artery is present, section B is the section before the main coronary artery and branch are separated, and section C is the section in which the main coronary artery and branch are completely separated.

The exact locations of these cross-sections in the computational model at the BS are illustrated in Fig. 4. A multi-faceted study was conducted on the distance between the ablation catheter and the coronary artery, considering the variability in cardiac tissue thickness among different populations. Studies have shown that patients with coronary BS implantation tend to have a greater epicardial fat thickness compared to the normal population^{43–45}.

The ablation effect of pulsed electric field ablation with a pulse voltage of 1000 V and a pulse width of 100 μ s is shown in Fig. 5A. In this simulation, the ablation catheter was positioned 1 mm from the coronary artery,

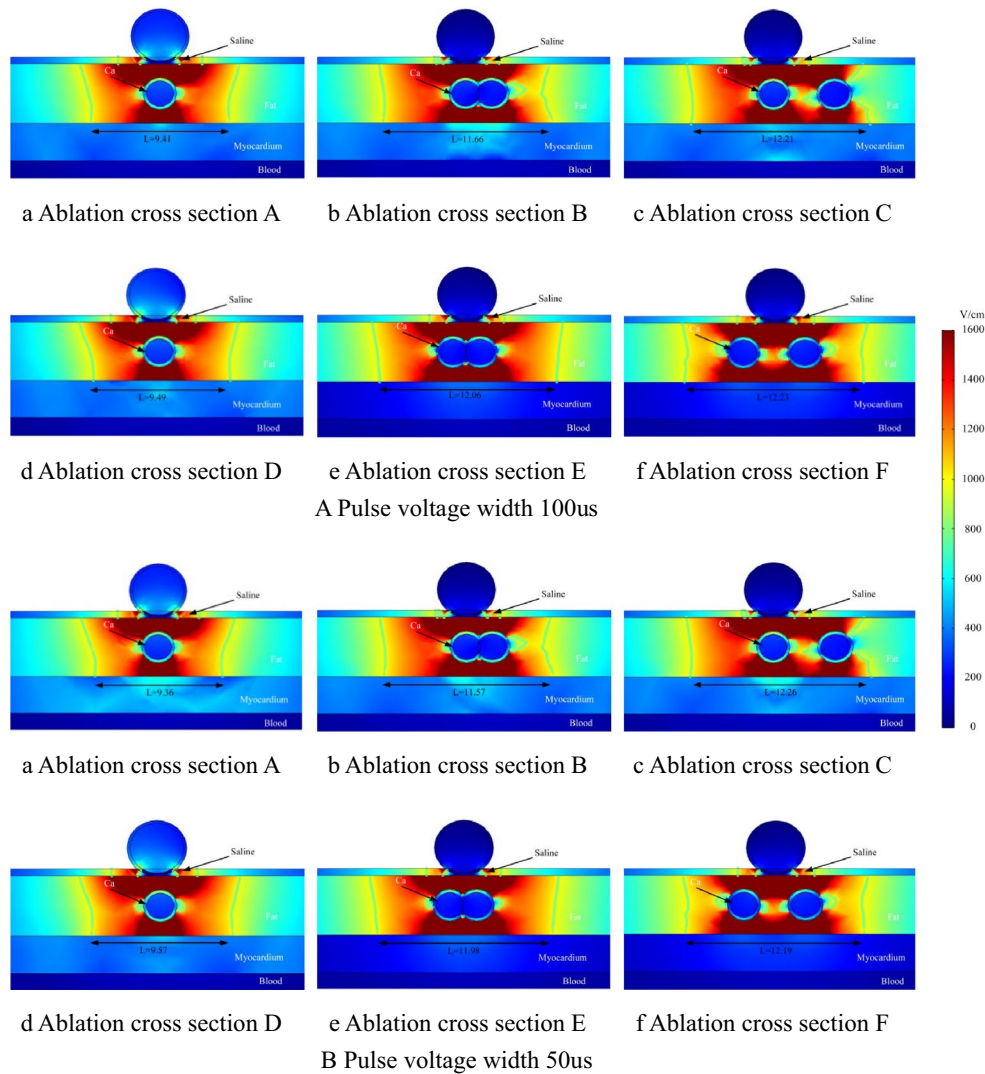
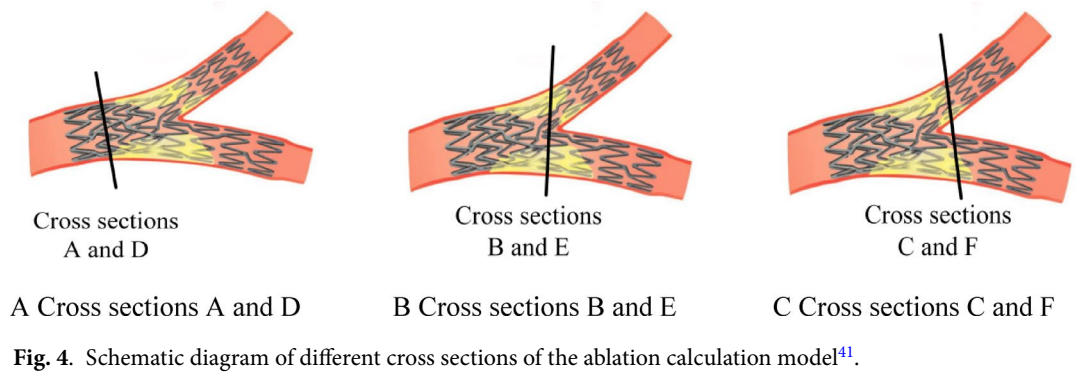


Fig. 5. No bifurcation stents inside the coronary artery, pulse voltage of 1000 V, and ablation catheter at a distance of 1 mm from the coronary artery.

and no BL was present. Computational model analysis showed that, regardless of the angle between the ablation catheter and the coronary artery, cold spots (regions with lower electric field values) and hot spots (regions with higher electric field values) appeared symmetrically on both sides of the coronary artery. Notably, the cold spot region was larger when there was no angle between the ablation catheter and the coronary artery than when an angle was present. This is likely due to the greater distance between the coronary artery and its branches in the

absence of an angle, as shown in Figs. 5Ab and 5Ae. The ablation region is wider in cross-sections where the main coronary artery and branches intersect at the computational model interface, as shown in Figs. 5Aa, 5Ab, and 5Ad, 5Ab. This phenomenon remains unchanged despite variations in the distance between the main branch and its branches, as indicated by Fig. 5B, 5Ac, and 5Ae, 5Af.

The ablation effect of pulsed electric field ablation with the ablation catheter at a distance of 1 mm from the coronary artery at a pulse width of 50 us is shown in Fig. 5B. In this simulation, no BL was produced in the coronary artery. Compared with Fig. 5A, we only changed the pulse voltage width to 50us in the computational simulation and found that the width of the pulsed electric field ablation region was almost unchanged in the two computational simulation results (the maximum difference was 0.09 mm, compared with Figs. 5Ab and 6Bb.), and the ablation region was restricted to the fat layer only, and no damage was produced to the myocardial layer. Damage. Similar to the results of Fig. 5A, when only the main coronary branch was present, the width of the ablation region was much smaller than that in the case of the simultaneous presence of the main branch and the branch (width of 9.41 mm in Fig. 5Aa, width of 11.66 mm in Fig. 5Ab, width of 9.36 mm in Fig. 5Ba, and width of 11.57 mm in Fig. 5Bb.). This indicates that changes in pulse voltage width do not cause changes in the width of the ablation region.

The ablation effect of pulsed electric field ablation at a pulse voltage of 1000 V and a pulse width of 100 us is shown in Fig. 6. In this simulation, the ablation catheter was 1.5 mm away from the coronary artery, and there was no BS inside the coronary artery. comparing Fig. 5 with Fig. 6, the change of the distance between the ablation catheter and the coronary artery had a limited effect on the ablation results, and the overall ablation trend of the ablation area did not change. The difference was greatest when there was an angle between the ablation catheter and the coronary artery (both main and branch coronary arteries were present in the ablation

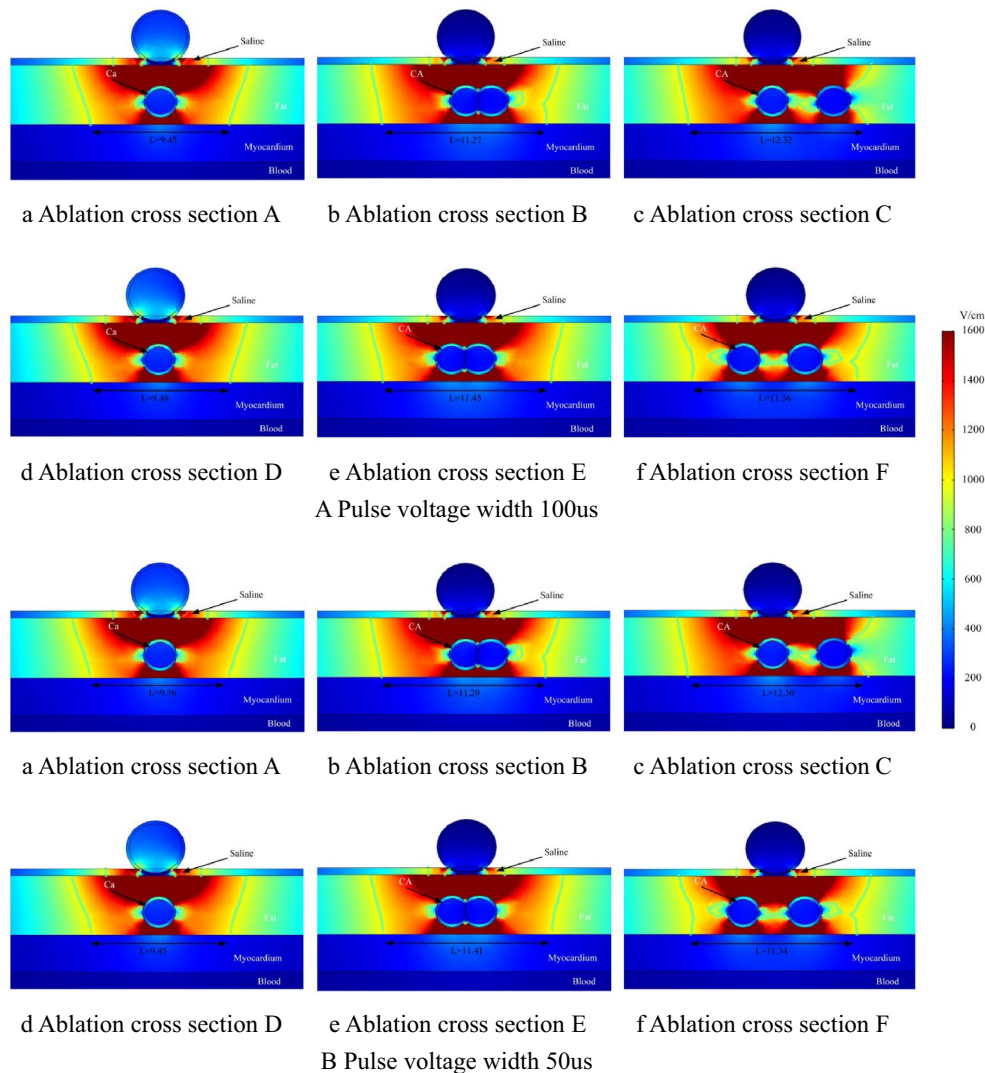


Fig. 6. No bifurcation stents inside the coronary artery, pulse voltage of 1000 V, and ablation catheter at a distance of 1.5 mm from the coronary artery.

cross-section) (Fig. 5Ae width 12.06 mm, Fig. 5Af width 12.23 mm, Fig. 6Ae width 11.45 mm, Fig. 6Af width 11.36 mm, with a maximum difference in the width of the ablated area of 0.61 mm and 0.77 mm, respectively).

In the presence of BS in the coronary arteries, we specifically analyzed the effect of BS on the presence of pulsed electric field ablation according to the previous classification. It is worth noting that we categorized such cases into four types in the present study similar to the above, respectively, and the ablation effect of pulsed electric field ablation at a pulse voltage of 1000 V and a pulse width of 100 us is shown in Fig. 7. In the present simulation, the ablation catheter was 1 mm from the coronary artery, and there was BS inside the coronary artery.

Similar to the previous findings the cold and hot spots in the ablation region do not change their positions due to the presence of BS. It is worth noting that the distortion of the electric field in the ablation region by the presence of BS is more obvious, comparing Fig. 7Ab with Fig. 5Ab, it can be concluded that the cold spots in the ablation region continue to expand when BS is present, and this manifestation results in the phenomenon that the value of the electric field in the intermediate region of the ablation is less than 1000 V/cm, which results in the reduction of the width of the ablation region (Fig. 5Ab width 11.66 mm, Fig. 9Ab width 10.68 mm.) The ablation effect of pulsed electric field ablation at a pulse voltage of 1000 V and a pulse width of 50 us is shown in Fig. 7B. In this simulation, the ablation catheter was 1 mm away from the coronary artery, and there was a BS inside the coronary artery. Comparing Fig. 7A with Fig. 7B, the change in the pulse voltage width had a small effect on the width of the ablation area, a phenomenon similar to the previous phenomenon in which there was no BS inside the coronary artery (the maximum difference in the width of the ablation area was 0.36 mm, which is derived from comparing Fig. 7Ac width 11.76 mm and Fig. 7Bc (width 12.13 mm).)

The ablation effect of pulsed electric field ablation at a pulse voltage of 1000 V and a pulse width of 100 us is shown in Fig. 8. In this simulation, the distance of the ablation catheter from the coronary artery is 1.5 mm,

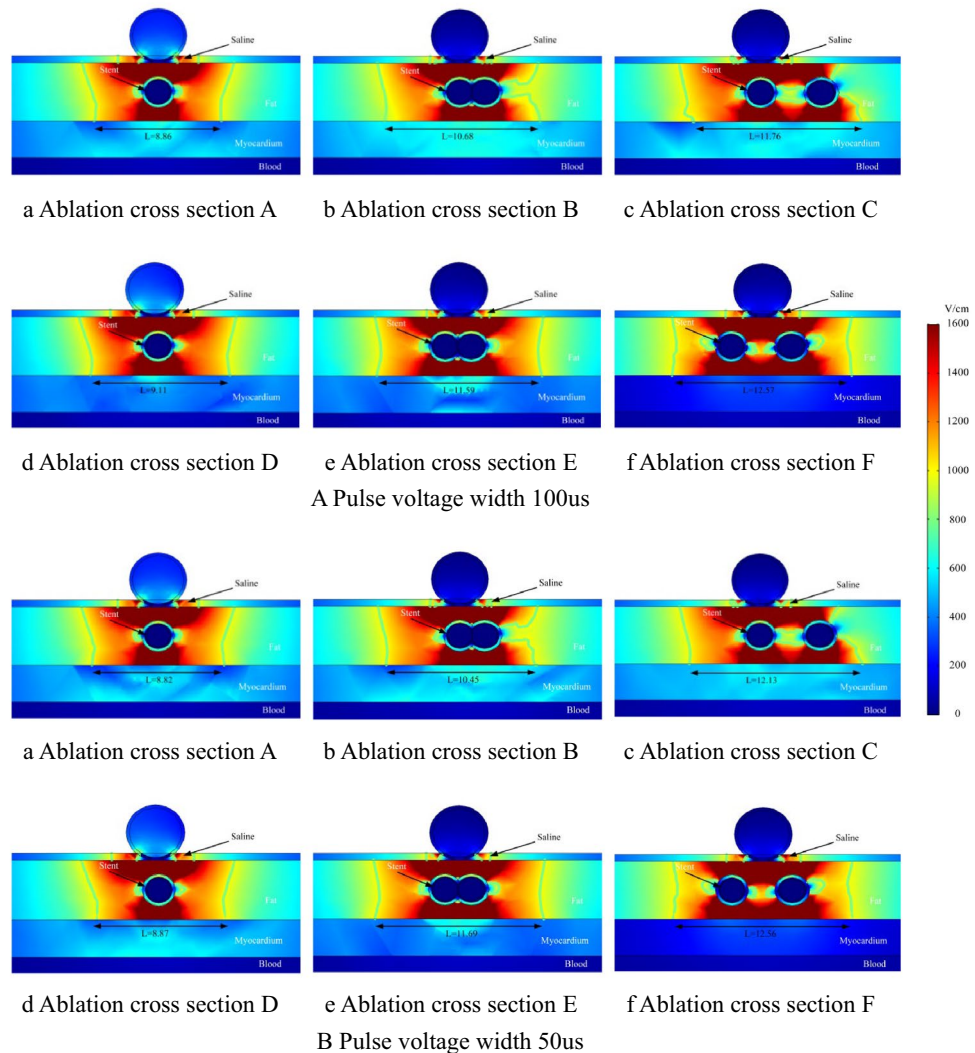


Fig. 7. Bifurcation stents inside the coronary artery with a pulse voltage of 1000 V. The distance between the ablation catheter and the coronary artery is 1 mm.

and there is BS inside the coronary artery. Compared with Fig. 7, we change the distance between the ablation catheter and the coronary artery in the computational simulation, and we can observe that in Fig. 8Ab, the cold spot area on the right side of the coronary artery becomes smaller, and the entire ablation area forms an encapsulated area, and the width of the ablation area has a large change (Fig. 7Ab width 10.68 mm, Fig. 8Ab width 11.31 mm, and the difference in the width of the ablation area is 0.63 mm). This ablation effect was similar to that of the previous BS-free ablation area in the intracoronary arteries, and therefore, this also suggests that the catheter can be discharged in multiple locations during BS pulse ablation to achieve a better ablation effect.

The ablation effect of pulsed electric field ablation at a pulse voltage of 1000 V and a pulse width of 50 μ s is shown in Fig. 8B. Comparing Fig. 8A with Fig. 8B, it can be concluded that changing only the pulse voltage width has less effect on the ablation area with the same ablation parameters, a phenomenon we mentioned above. Comparing Fig. 7, it can be obtained that the change in the distance between the ablation catheter and the coronary artery still led to the phenomenon that the cold spot region on the right side of the coronary artery became larger. With the same pulse ablation parameters, it seems that a larger distance between the ablation catheter and the BS also has a larger effect on the width of the ablation area. Comparing Figs. 7 and 8, in our three cross-sections taken from the computational model, Fig. 8 corresponds to a somewhat larger ablation width in each section than that of Fig. 7 (the maximum difference in the ablation region width is 0.89 mm, and a comparison of the width of Fig. 7Bb, 10.45 mm, with that of Fig. 8Bb yields a width of 11.34 mm).

The orthogonal test is an efficient experimental method, primarily used for multi-factor and multi-level experiments. Representative experimental groups can be selected using an orthogonal table to analyze the effects of each factor. During epicardial ablation, the effectiveness of the targeted region is primarily determined by the threshold of the electric field distribution. Therefore, we conducted an orthogonal test to better analyze the key factors influencing the ablation region.

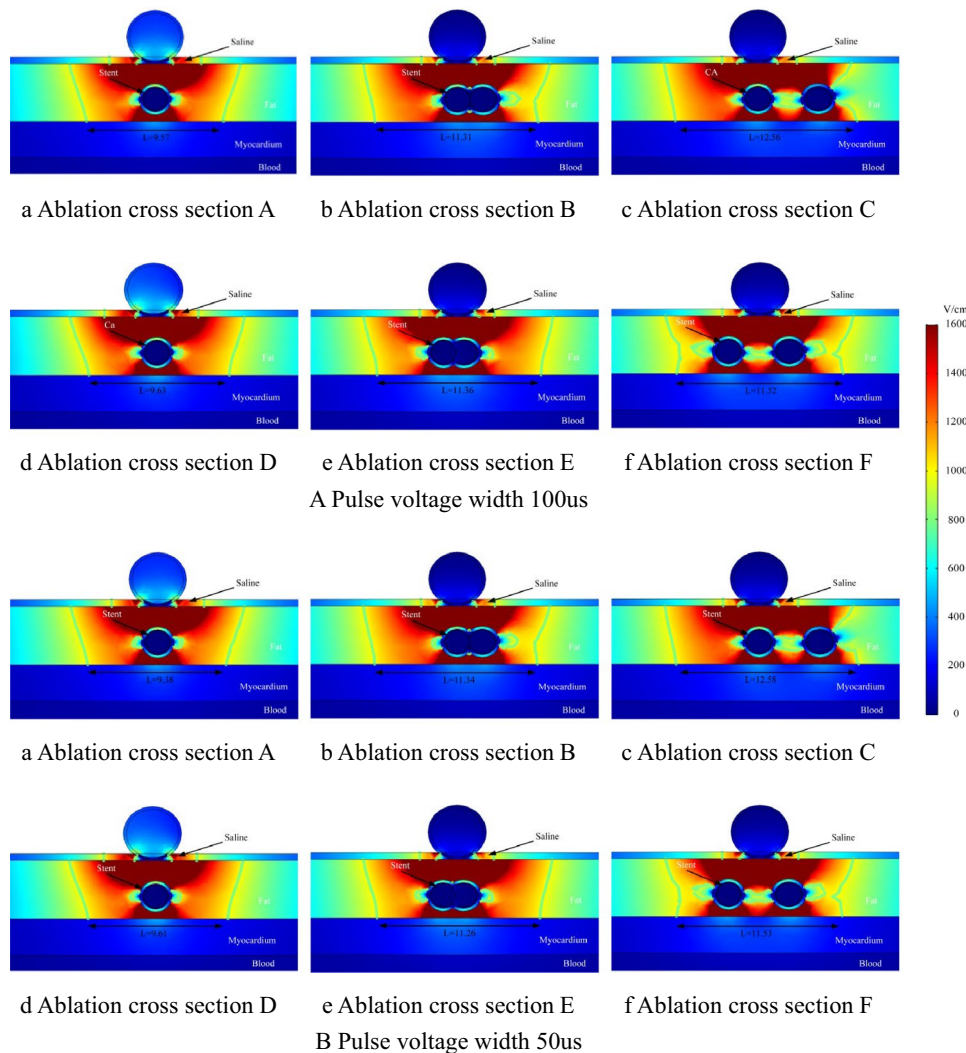


Fig. 8. Bifurcation stents inside the coronary artery with a pulse voltage of 1000 V. The distance between the ablation catheter and the coronary artery is 1.5 mm.

Experiment number	Stent (2 levels)	Angle (2 levels)	Distance (2 levels)	Cross-Sect. (3 levels)	Y-value
1	A ₁	B ₁	C ₁	D ₁	9.41
2	A ₁	B ₁	C ₂	D ₂	11.27
3	A ₁	B ₂	C ₁	D ₃	12.23
4	A ₁	B ₂	C ₂	D ₁	9.48
5	A ₂	B ₁	C ₁	D ₂	10.68
6	A ₂	B ₁	C ₂	D ₃	12.56
7	A ₂	B ₂	C ₁	D ₁	9.11
8	A ₂	B ₂	C ₂	D ₂	11.36
9	A ₁	B ₁	C ₁	D ₃	12.21
10	A ₁	B ₂	C ₂	D ₂	11.45
11	A ₂	B ₁	C ₂	D ₁	9.57
12	A ₂	B ₂	C ₁	D ₃	12.57

Table 3. Orthogonal test table of ablation effect.

Source	Sum of Squares (SS)	Degrees of Freedom (df)	Mean Square (MS)	F-value	P-value
Stent: A	0.003	1	0.003	0.090	0.774
Angle: B	0.021	1	0.021	0.563	0.481
Distance: C	0.355	1	0.355	9.601	0.021
Cross-section: D	18.569	2	9.284	250.861	0.000
Error	0.222	6	0.037		
Total	18.838	11			

Table 4. Table of ANOVA results.

In this study, we employed an orthogonal experimental design with four factors (bracket, angle, distance, and cross-section) and one outcome variable (ablation width). Table 3 presents the orthogonal test matrix used in this study. The ablation width (Y value) was obtained from simulation-derived calculations in the previous analysis.

In Table 3 stent (1 indicates no stent, 2 indicates stent), angle (1 indicates no angle of the ablation catheter to the main branch of the coronary artery, 2 indicates an angle of the ablation catheter to the main branch of the coronary artery), distance (1 indicates the ablation catheter to the coronary artery as 1 mm, 2 indicates the ablation catheter to the coronary artery as 1.5 mm), and cross-Sect. (1 indicates cross sections A and D, 2 indicates cross sections B and E, and 3 indicates cross sections C and F). Correlation calculations on the orthogonal experimental tables yielded Table 4.

We computed the sum of squares, mean squares, F-values, and p-values for each factor. Factor D ($F = 250.861$, $p < 0.005$) exhibits extremely high significance, indicating a strong effect on the ablation results. Factors A, B, and C, with low F-values and p-values well above 0.05, have minimal influence on the ablation results. Among factors A, B, and C, factor C has a p-value of 0.021, suggesting that it is the second most influential factor in this simulation. The sum of error squares in Table 4 is 0.222, corresponding to an error of approximately 1.18% relative to the total sum of squares (18.838). This small discrepancy indicates that our experimental data are highly stable and reliable.

Temperature distribution

In this computational simulation, the temperature variation in the ablation region is another focus of our study, and in this study, we measure the temperature for the selected ablation cross-section and also mark the maximum temperature in the ablation region. Similar to the electric field distribution study, in the study of temperature measurement in the ablation region, we use the same classification criteria, firstly into whether the BL site is installed with a BS or not, and for this lesion we perform a secondary classification into two types of ablation catheters and coronary arteries of 1 mm and 1.5 mm, respectively, which are computationally simulated firstly in the article. The ablation effect of pulsed electric field ablation at a pulse voltage of 1000 V and a pulse width of 100 us is shown in Fig. 9. In this analog simulation, the ablation catheter was 1 mm from the coronary artery and there was no BS inside the coronary artery.

In Fig. 9, it is shown that when the ablation area has both the presence of the main coronary artery and the branch, the change in the angle between the ablation catheter and the main branch has a greater effect on the temperature of the ablation area (Fig. 9Ac ablation area temperature 41.88 °C, Fig. 9Af ablation area temperature 40.52 °C). This indicates that the presence of coronary arteries has a large effect on the temperature variation in the ablation region. At the same time, similar to the ablation electric field distribution, there are cold and hot spots in the ablation region temperature, which can be obtained from the figure that the temperature of the

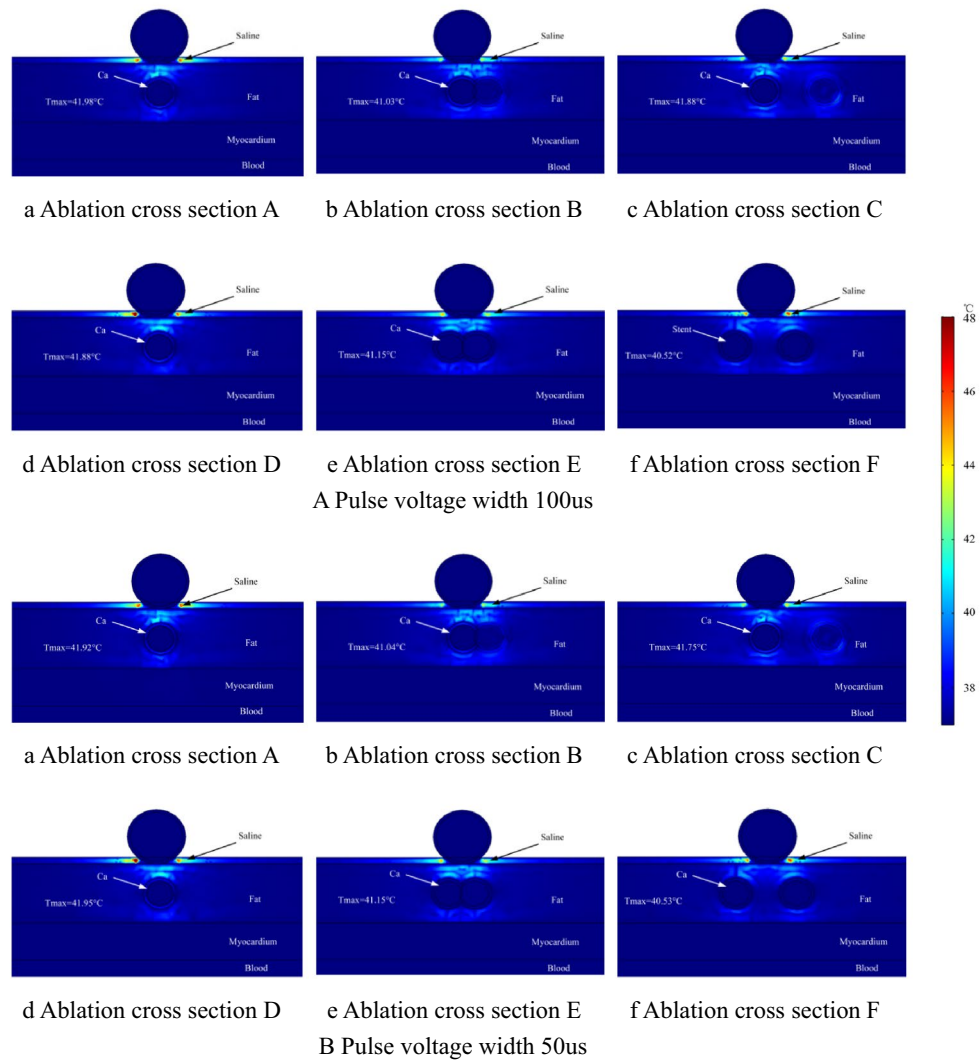


Fig. 9. No bifurcation stents inside the coronary artery, pulse voltage of 1000 V, and ablation catheter at a distance of 1 mm from the coronary artery.

upper and lower sides of the coronary artery is higher than that of the left and right sides, and this phenomenon does not change because of the angle between the ablation catheter and the main branch of the coronary artery.

Shown in Fig. 9B is a schematic of the ablation zone temperature compared with Fig. 9A where only the pulse voltage width was changed. Similar to the pulse voltage of 100 us, the change in the angle between the ablation catheter and the main coronary artery branch had a greater effect on the ablation region temperature when both the main coronary artery branch and the branch were present (Fig. 9Bc ablation region temperature 41.75 °C, Fig. 9Bf ablation region temperature 40.53 °C). It is worth noting that we performed the ablation voltage pulse width interpretation in the previous section. In the present study, no matter how the width of the pulse voltage was changed, the total pulse duration did not change, which led to no significant change in the ablation region temperature (the highest temperature in the ablation region was 41.98 °C and the lowest temperature was 40.52 °C).

Figure 10A shows the ablation effect of pulsed electric field ablation at a pulse voltage of 1000 V and a pulse width of 100 us. Figure 10B shows the ablation effect of pulsed electric field ablation at a pulse width of 50 us. In these two computational simulations, the ablation catheter was 1.5 mm away from the coronary artery, and there was no BS inside the coronary artery. comparing Figs. 9 and 10, we found that the distance between the ablation catheter and the coronary artery had a large effect on the temperature change of the ablation area, and when the distance between the ablation catheter and the coronary artery was 1 mm, the temperature of the corresponding cross-section in the ablation area was greater than that of the ablation catheter and the coronary artery at a distance of 1.5 mm.

When the distance between the ablation catheter and the coronary artery was 1 mm, the temperature of the corresponding cross-section in the ablation area was greater than that when the distance between the ablation catheter and the coronary artery was 1.5 mm. However, this temperature change did not produce thermal damage

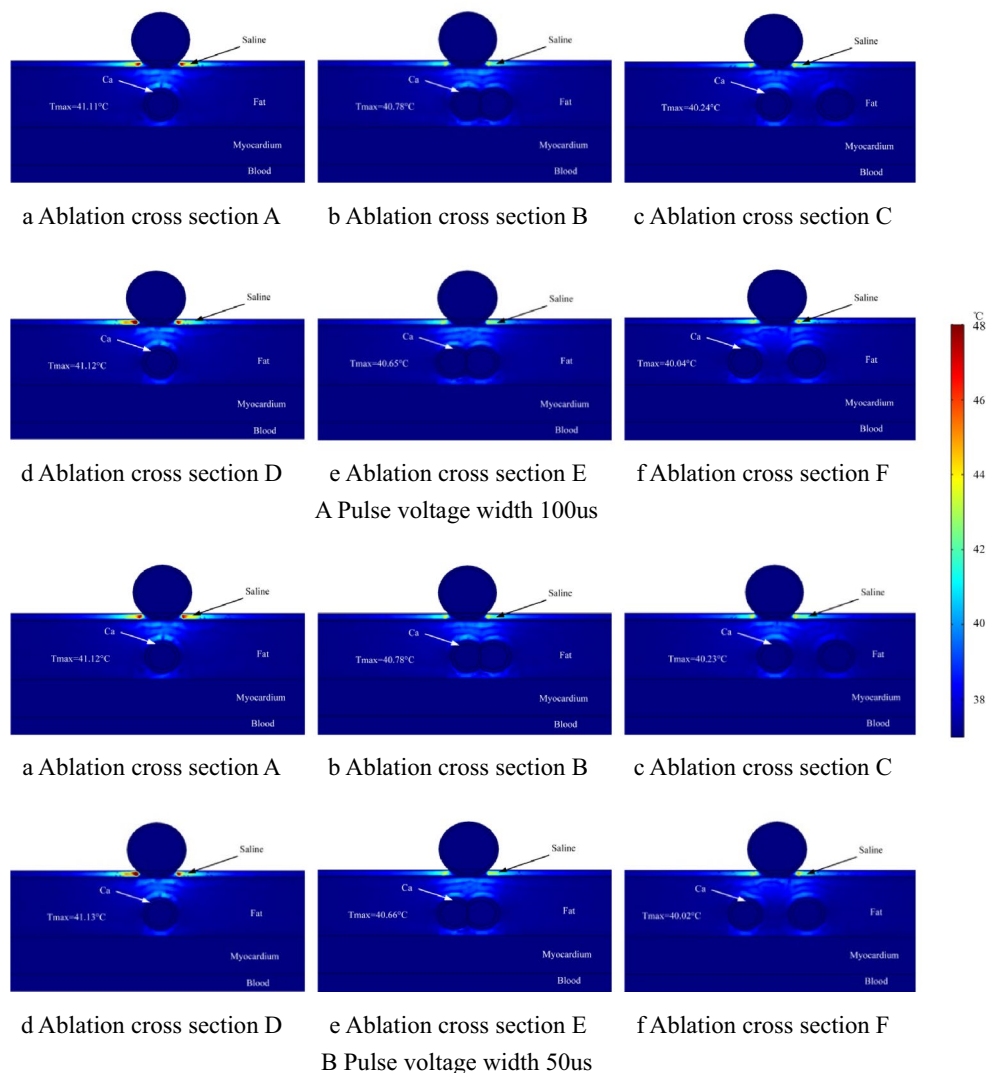


Fig. 10. No bifurcation stents inside the coronary artery, pulse voltage of 1000 V, and ablation catheter at a distance of 1.5 mm from the coronary artery.

to the tissue in the ablation region (maximum temperature of 41.98 °C, as shown in Fig. 9Aa). Comparing Figs. 10 A and 10B, it can be concluded that the temperature in the ablation region does not change significantly when the ablation parameter is changed only by the pulse width, and this conclusion does not change because of the distance between the ablation catheter and the coronary artery (the maximum difference is only 0.02 °C, as shown in Figs. 10Af and 10Bf.).

In the presence of BS in the coronary arteries, we specifically analyzed the effect of BS on the presence of pulsed electric field ablation according to the previous classification. Figure 11A shows the ablation effect of pulsed electric field ablation at a pulse voltage of 1000 V and a pulse width of 100 us. Figure 11B shows the ablation effect of pulsed electric field ablation at a pulse width of 50us. In this simulation, the ablation catheter was 1 mm away from the coronary artery, and BS was present inside the coronary artery.

As shown in Fig. 11A, the maximum temperature in the ablation region is 43.58 °C and the minimum temperature is 40.95 °C. It is worth noting that no matter in Fig. 11A and B, the cross-section of the maximum value of the ablation region temperature occurs consistently (as shown in Fig. 11Ad and Fig. 11Bd), and similar to the previous calculation and simulation results is that the change of the pulse voltage width does not cause a large change of the temperature of the ablation region, which may be in the case of because the total pulse length is the same, the ablation region is heated for the same amount of time, and therefore the ablation region temperature change trend is similar. In contrast to Fig. 9, the presence of BS exacerbates the increase of the ablation region temperature. However, the distribution of temperature in the ablation region did not change (the temperature maxima all occurred in the section of the ablation region containing only the main coronary artery branch).

Figure 12A shows the ablation effect of pulsed electric field ablation at a pulse voltage of 1000 V and a pulse width of 100 us. In this simulation, the ablation catheter was 1.5 mm away from the coronary artery, and at this

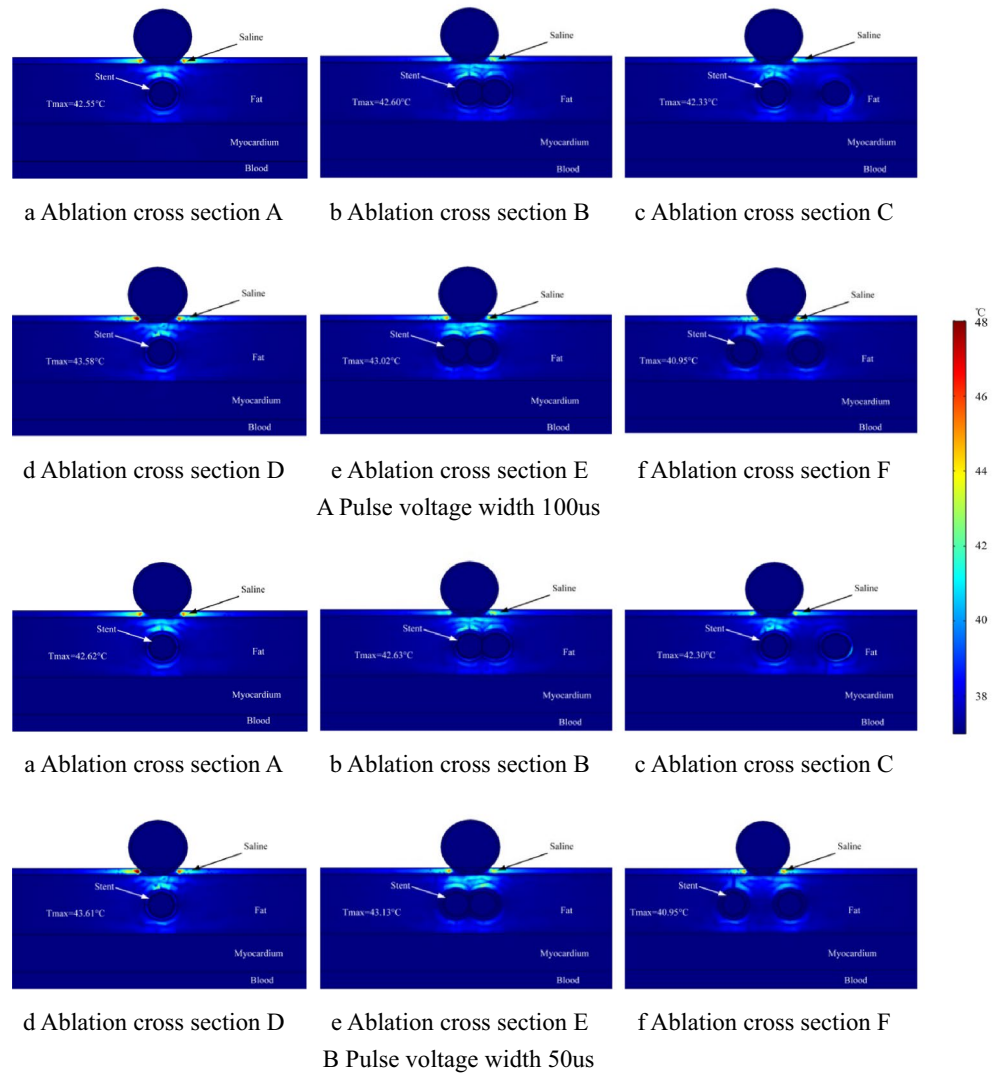


Fig. 11. Bifurcation stents inside the coronary artery with a pulse voltage of 1000 V. The distance between the ablation catheter and the coronary artery is 1 mm.

time, there was a BS inside the coronary artery. Comparing Figs. 11A and 12A, it can be concluded that when there is a BS inside the coronary artery, the distance between the ablation catheter and the BS has a large effect on the temperature of the ablation area (e.g., the temperature of Fig. 11Ad was 43.58°C , and the temperature of Fig. 12Ad was 41.47°C , and the temperature of both of them differed by 2.11°C due to the change of the distance). Change both temperatures differed by 2.11°C .). At the same time, when the ablation catheter was 1 mm away from the coronary artery, the temperature of the cross section corresponding to the ablation area was greater than that when the ablation catheter was 1.5 mm away from the coronary artery, and this change did not occur because of the difference in cross-section.

Figure 12B shows the ablation effect of pulsed electric field ablation at a pulse width of 50 μs . Similar to Fig. 12A, the ablation region temperature was similar at the same ablation cross-section, and the maximum difference between the two temperatures was only 0.02°C . This is also similar to what we have previously described, that the ablation region temperature does not change due to the change in pulse width when the total pulse duration is equal. Comparing Figs. 11B and 12B, it can be concluded that the maximum ablation region temperature occurs in the cross-section where only the main coronary artery branch is present. At the same time, as the distance between the ablation catheter and the coronary artery becomes larger, the ablation region temperature decreases accordingly, which may be due to the fact that the phenomenon of ablation region temperature increase caused by the BS is weakened due to the longer distance of the BS from the ablation catheter (the temperature of Fig. 11Bd is 43.61°C and the temperature of Fig. 12Bd is 41.46°C , which is a difference of 2.15°C .). This conclusion can be similarly drawn in Fig. 11A vs. Figure 12A, but this change in temperature does not cause tissue damage in the ablation region.

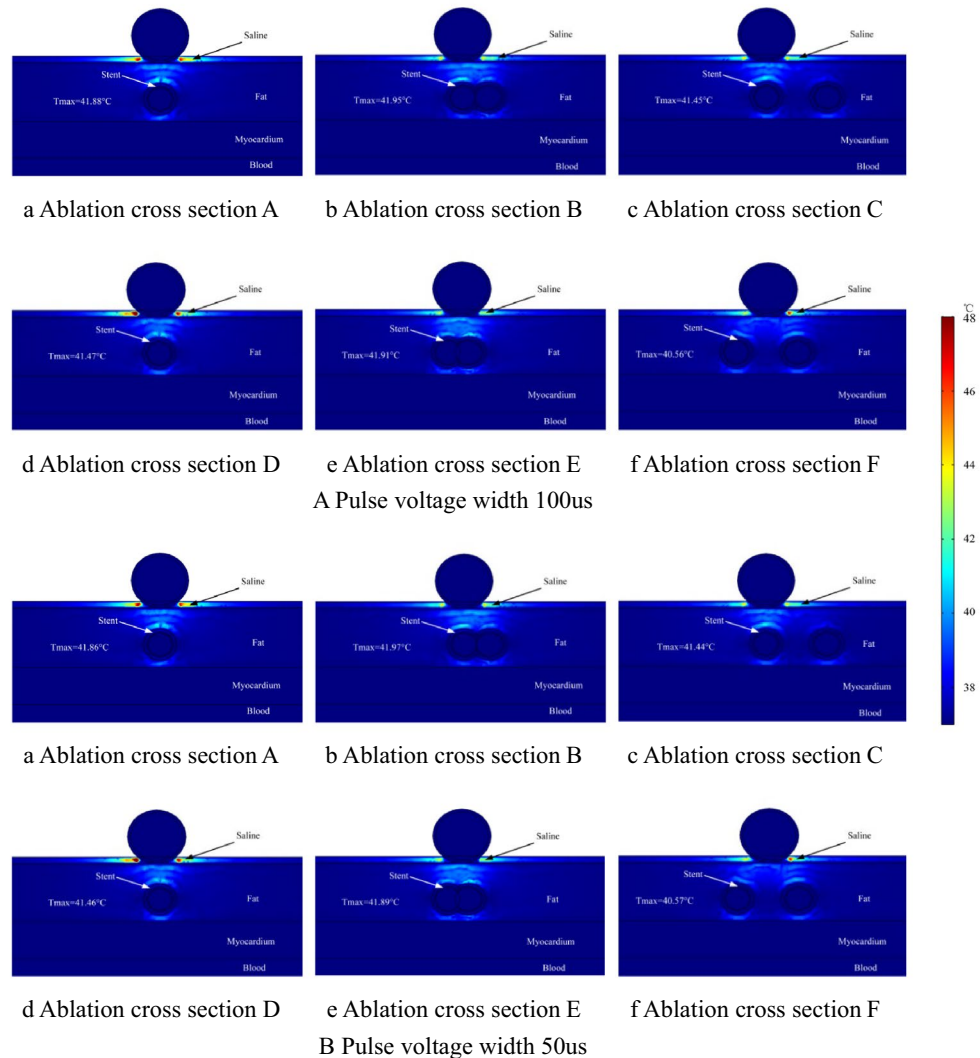


Fig. 12. Bifurcation stents inside the coronary artery with a pulse voltage of 1000 V. The distance between the ablation catheter and the coronary artery is 1.5 mm.

Discussion

Several clinical methods are available for arrhythmia treatment, including cryoablation and radiofrequency ablation. Compared to these, pulsed-field ablation for pulmonary vein isolation in atrial fibrillation reduces tissue damage in the ablation area (e.g., esophagus, phrenic nerve). Some studies have shown that the epicardial ganglion plays a key role in arrhythmia regulation, but fewer studies have focused on epicardial pulsed-field ablation for arrhythmia treatment^{46–49}. Therefore, we propose a computational simulation of ablation in BL patients, using a three-dimensional simplified model with multiple parameters and cross-sections.

Main findings

Pulsed electric field ablation has garnered significant interest for arrhythmia treatment due to its superior safety profile compared to other techniques such as cryoablation and radiofrequency ablation. However, fewer studies have focused on epicardial ablation for arrhythmia treatment. Recent studies have shown that epicardial ablation for arrhythmias may cause temperature increases in the target area due to the presence of bifurcation stents (BS) in coronary arteries. Researchers speculate that this warming effect is due to the unique properties of the metal^{29,50}. Researchers have also found that the presence of the ganglion plexus and coronary arteries during epicardial ablation significantly distorts the electric field distribution in the ablation region^{9,13,51}. However, to date, no studies have examined the electric field and temperature distribution in the ablation area for BL and BS in pulsed electric field ablation. This complex lesion may have a significant impact on arrhythmia treatment with epicardial pulsed electric field ablation. To the best of our knowledge, this is the first simulation study to model pulsed ablation based on BL. In this study, we employed three-dimensional modeling, multi-angle simulations of the ablation catheter and BL, and multi-parameter simulations of pulsed ablation parameters and the distance between the catheter and coronary stent. The main findings of this study include:

1. The presence of BS in the BL affects the area in which the cold spot exists, and when a BS is present, the cold spot on the coronary side may fail to form an effectively wrapped area (with an electric field value greater than 1,000 V/cm.).
2. When the main coronary artery in the ablation cross-section is present along with the branches, the cold spots in the ablation area will be linked together, thus creating a larger cold spot area (derived from Fig. 7.).
3. For the presence of only the main branch in the BL in the ablation region, the width of the effective ablation region (electric field value greater than 1000 V/cm) is narrower, which is independent of the presence or absence of the BS in the BL (as can be deduced from the graph A of the distribution of the electric field in the ablation region.).
4. The presence of the BS inside the BL has a small effect on the width of the ablation region in this cross-section, with a maximum difference of 0.7 mm between the two at the same pulse parameter (derived from Figs. 5 and 7.).
5. When BS is present inside the BL, the temperatures of the corresponding cross sections in the ablation region are somewhat elevated, which indicates that the BS has a contributing effect on the temperature in the ablation region (the maximum is 43.61 °C in the presence of BS, as shown in Fig. 11, and 41.98 °C in the absence of BS.).
6. The presence of both main and branch coronary arteries does not exacerbate the rise in temperature in the ablation area, which is related only to the distance between the ablation catheter and the coronary artery.

In this study, we conducted 3D computer modeling of BL to assess its effect on the pulsed ablation area. We categorized ablation targets based on the presence or absence of BS in the BL and found that BS did not significantly impact the overall ablation area. The difference in ablation area between models with and without BS under identical parameters was only 0.7 mm (compared to the bifurcation-free stent), as shown in Figs. 6 and 10. Furthermore, our results align with previous studies, showing that in computational simulations, the presence of BS did not alter the position of the pulsed-field ablation area, which remained primarily distributed directly beneath the ablation catheter. The distance between the ablation catheter and the coronary artery had no impact on the position of the ablation area (Figs. 10 and 11).

For the first time, we analyzed and compared the ablation effects of different cross-sections of the BS using a three-dimensional computational model. Our findings indicate that the width of the pulsed electric field ablation area varies significantly between computational models, depending on the presence or absence of coronary artery branches. When the ablation catheter was positioned 1 mm from the coronary artery, the maximum ablation gap between the two computational models was 2.25 mm (Fig. 5A). This ablation gap was independent of the catheter-to-artery distance, the angle between the ablation catheter and the coronary artery, and the presence of BS in BL. When the distance between the catheter and the artery increased to 1.5 mm, the maximum ablation gap between the two computational models was 1.93 mm (Fig. 6A). When an angle was introduced between the catheter and the artery, the maximum ablation gap increased to 2.57 mm (Fig. 6A). The maximum ablation gap reached 2.82 mm in the presence of BS (Fig. 7B). A review of previous studies suggests that this phenomenon may result from significant variations in coronary artery diameter.

For the first time, we systematically analyzed the effect of BS on pulsed electric field ablation in BL. We considered pulse voltage width, the distance between the ablation catheter and the coronary artery, and the angle between the ablation catheter and the main coronary artery branch as independent variables, while treating ablation region width and temperature distribution across different cross-sections as dependent variables. Within the same model, across different cross-sections, the ablation region width increased with the distance between the main coronary artery and its branches. Notably, this increase in pulsed electric field region width was not correlated with the previously defined dependent variables (e.g., 9.36 mm in Fig. 7Aa, 11.29 mm in Fig. 7Ab, and 12.30 mm in Fig. 7Ac). This trend remained consistent in the presence of BS (e.g., 9.38 mm in Fig. 12A, 11.34 mm in Fig. 12B, and 12.58 mm in Fig. 12C).

Our findings indicate that the angle between the ablation catheter and the main coronary artery branch influences the size of the cold spot region in the ablation area. In this study, when an angle was present, the main coronary artery branch was entirely enclosed within the ablation-limited region (Figs. 6 and 8). Therefore, during ablation, our findings highlight the importance of adjusting the position of the ablation catheter relative to the coronary artery to achieve the desired clinical outcome.

In our study, the BS within the BL had a slight effect on increasing the temperature in the ablation region. However, this effect was not significantly greater than that of a single intracoronary stent, suggesting that BS does not induce a complex coupling effect to elevate temperature. The maximum temperature recorded was 43.61 °C in the presence of BS (Fig. 11) and 41.98 °C in its absence (Fig. 9). In this simulation, the maximum temperature in the ablation region remained below 44 °C, which is well below the lethal threshold for biological tissues. Therefore, we conclude that this temperature is unlikely to cause thermal damage to biological tissues^{13,52}.

Additionally, we observed that as the distance between the ablation catheter and the coronary artery increased, the temperature in the ablation region decreased. This trend was independent of the presence of a BS in the BL (Figs. 9, 10, 11 and 12). In this simulation, when the ablation catheter was parallel to the main branch of the coronary artery, temperature variations within the same ablation region were minimal, with a maximum difference of 0.95 °C (Fig. 9A). However, when an angle was present between the catheter and the main coronary branch, temperature variations were more pronounced, reaching a maximum difference of 2.66 °C (Fig. 11B). Therefore, altering the catheter's position relative to the coronary artery does not significantly affect regions with large temperature variations. Additionally, we observed that thermal hotspots in the ablation region were primarily located on the upper and lower sides of the coronary arteries, independent of the presence of branches. Our calculations suggest that the simulation results may represent a worst-case scenario for clinical ablation procedures, as the catheter was positioned directly above the coronary artery during data simulation.

Finally, in the present study, we found that regions with ablation electric field values exceeding 1000 V/cm were primarily located in the adipose layer. This is due to the lower conductivity of adipose tissue compared to myocardial tissue, which causes fat to act as a barrier to electric field dispersion^{20,53}. Previous studies have demonstrated that fat hinders electric field distribution. Therefore, during epicardial ablation, increasing the catheter electrode release voltage may be required to achieve effective myocardial damage^{20,23,54}. In our study, the electrical conductivity of the simulated cardiac stents may be higher than that of actual coated and pharmacologic stents. However, although increased conductivity may amplify electric field distortion, the overall trend remains unchanged, as similar distortion occurs even in the absence of a stent.

The BS used in this computational simulation represents a simplified stent. In clinical applications, metal stents come in various shapes and materials, which may slightly influence the electric field distribution in the ablation target region. However, our study, which simulates the electric field distribution in the presence of BS, provides an important foundation for future research. Studies have shown that when the catheter electrode is near a metal stent, significant distortion occurs in the surrounding electric field. This finding supports the validity of our study under experimental conditions^{10,11}.

In this study, we quantitatively analyzed the electric field distribution in the targeted ablation region, but did not assess the temperature field. This is because, during ablation, tissue damage is primarily induced by the electric field distribution, and in our simulations, the temperature did not reach levels that would cause thermal injury. Our quantitative analysis revealed that the cross-sectional location of the coronary artery significantly influenced the width of the ablation region. This suggests that the presence of a BS in the coronary artery enhances the catheter's ablation effect compared to cases where only the main branch is present. In clinical practice, multiple ablations of regions with only the main branch may be required to achieve comparable ablation outcomes.

Calculations indicate that the distance between the ablation catheter and the coronary arteries plays a crucial role in the ablation effect. This factor is particularly important because studies have shown that cardiac tissue thickness varies among populations. Notably, patients with coronary artery disease tend to have a thicker tunica albuginea than the general population. Therefore, this factor should be considered when performing pulse ablation in this patient group^{43–45}. Our analysis showed that the other two factors had a minor effect on ablation outcomes. Future studies can verify this by increasing the number of experiments, thereby reducing error and enhancing statistical significance. In addition, to verify the reliability of the computational simulations. We performed a total impedance calculation for the computational model, and we obtained a total impedance of 202 Ω for the computational model, a value that is consistent with the clinical monitoring values, which further increases the reliability of the computational model⁵⁵.

Some researchers have found that symptoms of arterial spasm may occur during PFA ablation for arrhythmia. In our current study, the ablation catheter was near the coronary arteries, which may have further increased the rate of arterial spasm occurring during ablation. Our investigation found that this phenomenon is also present in other ablation modalities, and researchers have found that mitigation with nitroglycerin can cause arterial spasms^{56–59}. This simulation is an a priori study, and we have only calculated and simulated the electric field damage and temperature distribution, therefore, in practical application, we recommend avoiding too high field strength for ablation therapy. At the same time, in the process of ablation therapy, the changes in electrocardiogram and other data should be observed, which can be a progressive increase of ablation energy to avoid the occurrence of arterial spasm phenomenon.

In this simulation, we used the probe function that comes with the software to record the temperature change during the ablation in real-time. By analyzing the temperature data we found that the temperature of the ablation region increases when the ablation catheter releases the pulse voltage, and decreases when the ablation catheter stops releasing the voltage, which indicates that the temperature increase is generated by the release of pulse energy. Therefore, the use of reasonable pulse parameters will play an important role in increasing the temperature of the ablation area, and it is also important to show that reasonable pulse parameters will reduce the formation of gas bubbles during PFA ablation, which is clinically important for reducing the risk of gas embolism in PFA treatment⁶⁰.

Limitations

In this study, we conducted three-dimensional digital modeling of the BS. The radial cross-section of the main branch of the coronary artery was selected for measuring the electric field and heat distribution, serving as the basis for data analysis and comparison across different models. We did not analyze data from the axial interface of the bifurcation frame, which may have led to incomplete acquisition of electric field and heat distribution data in the ablation region. Consequently, cross-sectional data in the relevant BS region may have been underrepresented. Nevertheless, we conducted a detailed computational analysis of the ablation catheter and the main branch of the coronary artery. Additionally, we examined the same computational model at three distinct BS locations (e.g., the cross-sections in Figures A, B, and C). Therefore, from a physical perspective, our study holds significant clinical relevance. It is important to note that the data used in our computational simulations were not derived from epicardial solid experiments. Therefore, while our calculations should be interpreted with caution in clinical applications, the observed trends in ablation data remain valuable for reference.

In addition, we simplified the occlusion status of the coronary bifurcation lesion (BL) in our model. In clinical practice, medical staff usually perform balloon dilatation at the BL site to ensure a smooth and uniform vessel diameter. We referred to the previous literature and simplified the model after consulting with relevant clinical researchers, which did not have a significant impact on the trend of the study results^{13,14}. In our study, we used a myocardial lethality threshold of 1000 v/cm, which is greater than the myocardial lethality threshold for pulsed electric fields mentioned in most of the literature. This is because we found through extensive literature reading that the highest pulsed electric field myocardial lethality threshold of 1000v/cm mentioned in the current

literature is due to the pulse parameters, the experimental environment, the cell culture method, and the tissue properties^{42,61,62}. We recognize that this may cause a reduction in our description of the ablation damage range, but this does not have an impact on the relevant conclusions.

Conclusion

In this study, we assessed the impact of BS on pulsed electric field distribution and potential thermal effects through three-dimensional computational modeling. By comparing the ablation regions in different computational models with variables such as the distance between the ablation catheter and the coronary artery, the presence of BS at the BL, and the angle between the ablation catheter and the main coronary artery branch, we found that these variables did not affect the distribution of the electric field or temperature in the ablation region. Cold spots in both the electric field and temperature distribution appeared on the left and right sides of the coronary artery, as did the hot spots.

Additionally, we observed that the ablation region width decreased when only the main branch was present (cross-sections A and D in Fig. 4). This change was independent of ablation parameters and the angle between the ablation catheter and the main coronary artery branch, suggesting that the ablation region width is more sensitive to the presence of a branch^{9,13}. Finally, our computational simulations showed that BS did not significantly increase the temperature in the ablation region (Figures A–D in the electric field distribution graphs). This suggests that pulsed electric field ablation in the presence of BS does not cause unnecessary tissue damage, with a maximum recorded temperature of 43.61 °C.

Data availability

Data availability: The datasets used and/or analysed during the current study available from the corresponding author on reasonable request.

Received: 10 March 2025; Accepted: 4 July 2025

Published online: 14 July 2025

References

1. Verma, A. et al. Primer on pulsed electrical field ablation: Understanding the benefits and limitations[J]. *Circulation: Arrhythmia Electrophysiol.* **14** (9), e010086 (2021).
2. Xie, F. et al. Irreversible electroporation ablation for atrial fibrillation: status and Challenges[J]. *Cardiol. Discovery.* **2** (01), 41–50 (2022).
3. Chun, K. R. J. et al. State-of-the-art pulsed field ablation for cardiac arrhythmias: ongoing evolution and future perspective[J]. *Europace.* **26** (6), euae134 (2024).
4. Reddy, V. Y. et al. Pulsed field or conventional thermal ablation for paroxysmal atrial fibrillation[J]. *N. Engl. J. Med.* **389** (18), 1660–1671 (2023).
5. Russo, A. M. Pulsed field ablation: is it better than conventional thermal ablation for treatment of atrial Fibrillation?[J]. *Circulation* **147** (19), 1433–1435 (2023).
6. Könemann, H. et al. Spotlight on the 2022 ESC guideline management of ventricular arrhythmias and prevention of sudden cardiac death: 10 novel key aspects[J]. *Europace* **25** (5), euad091 (2023).
7. Shen, M. J. & Zipes, D. P. Role of the autonomic nervous system in modulating cardiac arrhythmias[J]. *Circul. Res.* **114** (6), 1004–1021 (2014).
8. O'Brien, B. et al. Cardioneuroablation using epicardial pulsed field ablation for the treatment of atrial fibrillation[J]. *J. Cardiovasc. Dev. Disease.* **10** (6), 238 (2023).
9. González-Suárez, A. et al. Pulsed electric field ablation of epicardial autonomic ganglia: computer analysis of monopolar electric field across the tissues involved[J]. *Bioengineering* **9** (12), 731 (2022).
10. Scheffer, H. J. et al. The influence of a metal stent on the distribution of thermal energy during irreversible electroporation[J]. *PLoS One.* **11** (2), e0148457 (2016).
11. Månsson, C., Nilsson, A. & Karlson, B. M. Severe complications with irreversible electroporation of the pancreas in the presence of a metallic stent: a warning of a procedure that never should be performed[J]. *Acta Radiol. Short. Rep.* **3** (11), 2047981614556409 (2014).
12. Hogenes, A. M. et al. te Riet og Scholten G A., Effect of irreversible electroporation parameters and the presence of a metal stent on the electric field line pattern[J]. *Scientific reports*, 10(1): 13517. (2020).
13. González-Suárez, A. et al. In Silico modelling to assess the electrical and thermal disturbance provoked by a metal intracoronary stent during epicardial pulsed electric field ablation[J]. *J. Cardiovasc. Dev. Disease.* **9** (12), 458 (2022).
14. González-Suárez, A. et al. *Full Torso and limited-domain Computer Models for Epicardial Pulsed Electric Field ablation*[J]221106886 (Computer Methods and Programs in Biomedicine, 2022).
15. Gómez-Barea, M., García-Sánchez, T. & Ivorra, A. A computational comparison of radiofrequency and pulsed field ablation in terms of lesion morphology in the cardiac chamber[J]. *Sci. Rep.* **12** (1), 16144 (2022).
16. Silingardi, R. et al. Bifurcated coronary stents for infrapopliteal angioplasty in critical limb ischemia[J]. *J. Vasc. Surg.* **57** (4), 1006–1013 (2013).
17. Sánchez-Quintana, D. et al. Left atrial anatomy relevant to catheter ablation[J]. *Cardiol. Res. Pract.* **2014** (1), 289720 (2014).
18. Padmanabhan, D. et al. Electroporation of epicardial autonomic ganglia: safety and efficacy in medium-term canine models[J]. *J. Cardiovasc. Electrophys.* **30** (4), 607–615 (2019).
19. Yokokawa, M. et al. Impact of mitral isthmus anatomy on the likelihood of achieving linear block in patients undergoing catheter ablation of persistent atrial fibrillation[J]. *Heart Rhythm.* **8** (9), 1404–1410 (2011).
20. Gasperetti, A. et al. Determinants of acute irreversible electroporation lesion characteristics after pulsed field ablation: the role of voltage, contact, and adipose interference[J]. *Europace* **25** (9), euad257 (2023).
21. Di Biase, L. et al. Application repetition and electrode–tissue contact result in deeper lesions using a pulsed-field ablation circular variable loop catheter[J]. *Europace* **26** (9), euae220 (2024).
22. Irastorza, R. M. et al. Differences in applied electrical power between full thorax models and limited-domain models for RF cardiac ablation[J]. *Int. J. Hyperth.* **37** (1), 677–687 (2020).
23. Sano, M. B., Fan, R. E. & Xing, L. Asymmetric waveforms decrease lethal thresholds in high frequency irreversible electroporation therapies[J]. *Sci. Rep.* **7** (1), 40747 (2017).
24. Pan, C., Han, Y. & Lu, J. Structural design of vascular stents: A review[J]. *Micromachines* **12** (7), 770 (2021).

25. Khairulin, A., Kuchumov, A. G. & Silberschmidt, V. V. *In Silico Model of Stent Performance in multi-layered Artery Using 2-way fluid-structure Interaction: Influence of Boundary Conditions and Vessel length*[J]255108327 (Computer Methods and Programs in Biomedicine, 2024).
26. Suárez, A. G., Hornero, F. & Berjano, E. J. Mathematical modeling of epicardial RF ablation of atrial tissue with overlying epicardial fat[J]. *open. Biomedical Eng. J.* **4**, 47–55 (2010).
27. Tungjikusolmun, S. et al. Guidelines for predicting lesion size at common endocardial locations during radio-frequency ablation[J]. *IEEE Trans. Biomed. Eng.* **48** (2), 194–201 (2001).
28. Anjaneyulu, A. et al. Evaluation of left main coronary artery stenosis by transthoracic echocardiography[J]. *J. Am. Soc. Echocardiogr.* **21** (7), 855–860 (2008).
29. González-Suárez, A. & Berjano, E. Comparative analysis of different methods of modeling the thermal effect of Circulating blood flow during RF cardiac ablation[J]. *IEEE Trans. Biomed. Eng.* **63** (2), 250–259 (2015).
30. Sheehan, M. C. & Srimathveeravalli, G. Pulsed electric fields. Principles and Technologies for Electromagnetic Based Therapies. In Principles and Technologies for Electromagnetic Energy Based Therapies; Prakash, P., Srimathveeravalli, G., Eds.; Elsevier Academic Press: Cambridge, MA, USA, ; pp. 71–106. ISBN 9780128205945. (2021).
31. Ding, L. et al. Treatment planning optimization in irreversible electroporation for complete ablation of variously sized cervical tumors: a numerical study[J]. *J. Biomech. Eng.* **143** (1), 014503 (2021).
32. Sano, M. B. et al. Bursts of bipolar microsecond pulses inhibit tumor growth[J]. *Sci. Rep.* **5** (1), 14999 (2015).
33. Abraham, J. P. & Sparrow, E. M. A thermal-ablation bioheat model including liquid-to-vapor phase change, pressure-and necrosis-dependent perfusion, and moisture-dependent properties[J]. *Int. J. Heat Mass Transf.* **50** (13–14), 2537–2544 (2007).
34. Neal, I. I. R. E. et al. Experimental characterization and numerical modeling of tissue electrical conductivity during pulsed electric fields for irreversible electroporation treatment planning[J]. *IEEE Trans. Biomed. Eng.* **59** (4), 1076–1085 (2012).
35. Zang, L. et al. Investigate the relationship between pulsed field ablation parameters and ablation outcomes. *J. Interv. Card. Electrophysiol.* <https://doi.org/10.1007/s10840-024-01872-1> (2024).
36. Zhao, Y. et al. Characterization of conductivity changes during high-frequency irreversible electroporation for treatment planning[J]. *IEEE Trans. Biomed. Eng.* **65** (8), 1810–1819 (2017).
37. Fang, Z. et al. Irreversible electroporation enhanced by radiofrequency ablation: an in vitro and computational study in a 3D liver tumor model[J]. *Ann. Biomed. Eng.* **49** (9), 2126–2138 (2021).
38. Gabriel, C., Peyman, A. & Grant, E. H. Electrical conductivity of tissue at frequencies below 1 MHz[J]. *Phys. Med. Biol.* **54** (16), 4863 (2009).
39. Pérez, J. J., Ewertowska, E. & Berjano, E. Computer modeling for radiofrequency bipolar ablation inside ducts and vessels: relation between pullback speed and impedance progress[J]. *Lasers Surg. Med.* **52** (9), 897–906 (2020).
40. Gopalakrishnan, J. A mathematical model for irrigated epicardial radiofrequency ablation[J]. *Ann. Biomed. Eng.* **30**, 884–893 (2002).
41. Antoniadis, A. P. et al. Biomechanical modeling to improve coronary artery bifurcation stenting: expert review document on techniques and clinical implementation[J]. *Cardiovasc. Interventions.* **8** (10), 1281–1296 (2015).
42. Avazzadeh, S. et al. Establishing irreversible electroporation electric field potential threshold in a suspension in vitro model for cardiac and neuronal cells[J]. *J. Clin. Med.* **10** (22), 5443 (2021).
43. Gruzdeva, O. et al. Relationships between epicardial adipose tissue thickness and adipo-fibrokinase indicator profiles post-myocardial infarction[J]. *Cardiovasc. Diabetol.* **17**, 1–11 (2018).
44. Matloch, Z. et al. The role of inflammation in epicardial adipose tissue in heart diseases[J]. *Curr. Pharm. Design.* **24** (3), 297–309 (2018).
45. Rhee, T. M. et al. Association between epicardial adipose tissue thickness and parameters of target organ damage in patients undergoing coronary angiography[J]. *Hypertens. Res.* **42** (4), 549–557 (2019).
46. Wittkampf, F. H. M., van Es, R. & Neven, K. Electroporation and its relevance for cardiac catheter ablation[J]. *JACC: Clin. Electrophysiol.* **4** (8), 977–986 (2018).
47. De Potter, T. et al. Ultra-low temperature cryoablation for atrial fibrillation: primary outcomes for efficacy and safety: the cryocure-2 study[J]. *Clin. Electrophysiol.* **8** (8), 1034–1039 (2022).
48. Andrade, J. G. et al. Progression of atrial fibrillation after cryoablation or drug therapy[J]. *N. Engl. J. Med.* **388** (2), 105–116 (2023).
49. Koruth, J. S. et al. Endocardial ventricular pulsed field ablation: a proof-of-concept preclinical evaluation[J]. *EP Europace.* **22** (3), 434–439 (2020).
50. Stewart, M. T. et al. Safety and chronic lesion characterization of pulsed field ablation in a Porcine model[J]. *J. Cardiovasc. Electrophys.* **32** (4), 958–969 (2021).
51. Mohanty, S. et al. IS IT PREVENTABLE?[J]. *J. Am. Coll. Cardiol.* **83** (13_Supplement), 59–59 (2024).
52. Haines, D. E. Letter by Haines regarding article, direct measurement of the lethal isotherm for radiofrequency ablation of myocardial tissue[J]. *Circulation: Arrhythmia Electrophysiol.* **4** (5), e67–e67 (2011).
53. Wang, Z. et al. Effect of fat layer thickness on the ablation area in pulsed electric field ablation[C]//International Conference on Future of Medicine and Biological Information Engineering (MBIE 2024). SPIE, 13270: 342–350. (2024).
54. Meckes, D. et al. Pulsed-field ablation: computational modeling of electric fields for lesion depth analysis[J]. *Heart Rhythm.* **02** (4), 433–440 (2022).
55. Kitamura, T. et al. Usefulness of epicardial impedance evaluation for epicardial mapping and determination of epicardial ablation site for ventricular tachycardia: A pilot study[J]. *J. Cardiovasc. Electrophys.* **29** (1), 138–145 (2018).
56. Reddy, V. Y. et al. Coronary arterial spasm during pulsed field ablation to treat atrial fibrillation[J]. *Circulation* **146** (24), 1808–1819 (2022).
57. Hachisuka, M. et al. Perioperative coronary artery spasms in patients undergoing catheter ablation of atrial fibrillation. *J. Interv. Card. Electrophysiol.* **64**, 77–83. <https://doi.org/10.1007/s10840-021-01089-6> (2022).
58. Ladejobi, A. et al. Effects of pulsed electric fields on the coronary arteries in swine[J]. *Circulation: Arrhythmia Electrophysiol.* **15** (10), e010668 (2022).
59. Yajima, K. et al. Coronary artery spasm during cryoballoon ablation in a patient with atrial fibrillation[J]. *Intern. Med.* **57** (6), 819–822 (2018).
60. Mahnič-Kalamiza, S. et al. Elucidating the mechanisms of microbubble formation in intracardiac pulsed field ablation[J]. *Electrochim. Acta.* **497**, 144550 (2024).
61. Kos, B. et al. Determination of lethal electric field threshold for pulsed field ablation in ex vivo perfused Porcine and human hearts[J]. *Front. Cardiovasc. Med.* **10**, 1160231 (2023).
62. Miklavčič, D. et al. Biophysics and electrophysiology of pulsed field ablation in normal and infarcted Porcine cardiac ventricular tissue[J]. *Sci. Rep.* **14** (1), 32063 (2024).

Author contributions

Author contributions: Zhen Wang and Jingyang Sun for experimental conceptualization and first draft writing; Jie Zhang, Yulai Yan, and Fengqi Xuan for documentation and data analysis; Lisheng Xu, Ming Liang, and Yaling Han for technical guidance and review.

Funding

This research was funded by [The Open Project of the Central Logistics Support Department] grant number [BLB18C015]; [Science and Technology Program of Liaoning Provincial] grant number [2022JH2/101500017] and [Xingliao Talent Program of Liaoning Province] grant number [XLYC2203095].

Declarations

Competing interests

The authors declare no competing interests.

Additional information

Correspondence and requests for materials should be addressed to J.S. or Y.H.

Reprints and permissions information is available at www.nature.com/reprints.

Publisher's note Springer Nature remains neutral with regard to jurisdictional claims in published maps and institutional affiliations.

Open Access This article is licensed under a Creative Commons Attribution-NonCommercial-NoDerivatives 4.0 International License, which permits any non-commercial use, sharing, distribution and reproduction in any medium or format, as long as you give appropriate credit to the original author(s) and the source, provide a link to the Creative Commons licence, and indicate if you modified the licensed material. You do not have permission under this licence to share adapted material derived from this article or parts of it. The images or other third party material in this article are included in the article's Creative Commons licence, unless indicated otherwise in a credit line to the material. If material is not included in the article's Creative Commons licence and your intended use is not permitted by statutory regulation or exceeds the permitted use, you will need to obtain permission directly from the copyright holder. To view a copy of this licence, visit <http://creativecommons.org/licenses/by-nc-nd/4.0/>.

© The Author(s) 2025